

PROBABILITY OF DETECTION AND LIKELIHOOD: APPLICATION TO SPACE OBJECT OBSERVATION

F. Sanson⁽¹⁾ and C. Frueh⁽²⁾

⁽¹⁾200 Avenue de la Vieille Tour, 33405 Talence, France, Email: francois.sanson@inria.fr

⁽²⁾701 W. Stadium Ave. West Lafayette, IN 47907-2045, Email: cfrueh@purdue.edu

ABSTRACT

Charged Couple Device (CCD) technology is widely used in various scientific measurement contexts. CCD equipped cameras have revolutionized astronomy and space related optical telescope measurements in recent years, they are also widely used in electroscopic measurements. Even though CCD technology has dramatically improved since their initial deployment, measurements are necessarily never perfect and corrupted by noise. The probability of detection and likelihood are crucial statistical measures to properly design experiments, observation setup and in order to employ further mathematical methods for the data exploitation such as e.g. multi-target tracking methods. In the application to the observation of resident space objects in the near Earth space, noise sources include the sky background, atmospheric effects, besides the noise generated by the sensor itself. Previous attempts to correctly characterize the Signal to Noise ratio for star observations (Newberry and Merline et al.) have been revisited and adapted for the application of near Earth object observations and high precision measurements, leading to a modified CCD equation. In a second step, the probability of detection and likelihood, the object position uncertainty are rigorously derived. The results can readily be applied to CCD measurements.

Key words: optical observation, space object tracking, uncertainty quantification.

1. INTRODUCTION

Since its introduction in the early seventies, Charged Couple Device (CCD) technology revolutionized optical measurements in various scientific fields. For space object observations and tracking, CCDs typically yield non-resolved images that do not expose any details of the object of interests. In addition, noise generated by the detector itself and the image background, corrupts the object image; it blurs the object trace and raises the background level to varying values different from zero. As the object of interest only occupies a few pixels on non-resolved noisy images, even detection itself can be

extremely challenging, especially when object images are faint relative to the background. In any cases, being able to a priori estimate the probability of detection and the uncertainty in the object position, the so-called likelihood are a direct input parameter for the design of observation scenarios, campaigns and the choice of the correct instrument to begin with. The space object detection and tracking algorithms have been developed in [DFHC15, MDF15, DHF⁺15, CF08]; those methods rely on statistical input parameters of the probability of detection and likelihood.

Precise object position can be extracted from non resolved images by fitting a multi-variate Gaussian surface to the signal [HKD07]. As those observations are inevitably noisy one can only get imprecise knowledge of the space object position and motion. Estimation of the noise for star observations with a CCD detector have already been studied by [MH95, New91]. However for space objects such as space debris, some assumptions made in [MH95] and [HD08] may no longer be valid and alternative noise quantification models have to be developed. The methods have been revisited and been adapted for the nowadays higher precision requirements. Preliminary research has been published in [SF15]. A more extensive treatment of the topic is currently under review in [SF16a] and [SF16b]

2. ESTIMATION OF THE SIGNAL-TO-NOISE RATIO (SNR)

Traditionally, the Signal to Noise Ratio (SNR) is referred to as the CCD equation. Three different versions of the CCD equation are compared here: the classical as in [Tie93], Merline's improved [New91, MH95] and our improved derivation formulation. The classical CCD equation, Merline improves upon taking the process of the background determination into account. In our new derivation, the mismodeling of the truncation noise is assessed. Furthermore, the correlation of background and object trace pixels is taken into account, and ambiguous pixels as they often occur in faint sources are accounted for. For a more detailed derivation of the CCD equation please refer to [SF16a].

The basis of all three derivations is that the electron emission after absorption excited by the incoming photons is modelled by a Poisson random variable (hypothesis 1). This is true for the signals from the object $S_{\text{obj},i}$ and $S_{\text{S},i}$. Furthermore the dark noise, coming from spurious electron emission from the system, is also modelled as a Poisson variable $N_{\text{D},i}$. The following notation is used:

- n_{pix} is the number of pixels the signal is spread over
- $S_{\text{obj},i}$ the number of electrons emitted after absorption of photons emitted or reflected by the object for the pixel i . It is a Poisson random variable of parameter $\lambda_{\text{obj},i}$
- $S_{\text{S},i}$ the number of electrons emitted after absorption of photons emitted by background sources (e.g. stars) for the pixel i . It is a Poisson random variable of parameter $\lambda_{\text{S},i}$
- D_i the number of spurious electrons emitted for the pixel i (dark noise). It is a Poisson random variable of parameter $\lambda_{\text{D},i}$
- R_i the number of electrons introduced by the read out process per pixel i . It is modelled as a Gaussian distribution [MH95, Mas92].
- U_i is the number of electrons for the pixel i that are introduced by the limited CCD resolution. It is modelled by uniform distribution in [MH95, New91], while in this work its exact distribution is derived.

As noise generation is unpredictable in a CCD, the previous terms are seen as random variables.

The SNR is defined as the expectation value of the signal of interest divided by the standard deviation of the noise. The signal of interest is in our case, the object signal, that is the trace that the object leaves on the detector. It is spread over a number of pixels n . It is assumed to be well represented as a Poisson random variable. The signal S and its expectation value can hence be written as:

$$S = \sum_i^{n_{\text{pix}}} S_{\text{obj},i} \quad S^* := E[S] = \sum_i^{n_{\text{pix}}} \lambda_{\text{obj},i}, \quad (1)$$

In the classical and in the derivation of Merline of the CCD equation is assumed that the number n_{pix} of object pixels is exactly known (hypothesis 8).

The noise is defined as the variance of the sum of the object signal S together with the noise sources. For the i^{th} pixel, the noise sources consist of the celestial and sky background sources $S_{\text{S},i}$, such as stars, and other light sources, such as the zodiac light and other sources, that contribute to a non-zero photo background. Furthermore, the dark noise, D_i , of the detector, and the read out noise R_i , of the detector contribute to the noise of the CCD output. The realizations of both are influenced by the temperature of the detector. Furthermore, because CCDs have limited resolution not every single electron

can be reported. Inevitably there is a truncation noise introduced U_i . Then the total noisy CCD output is:

$$S_{\text{CCD}} = \sum_i^{n_{\text{pix}}} S_{\text{obj},i} + \sum_i^{n_{\text{pix}}} S_{\text{S},i} + \sum_i^{n_{\text{pix}}} D_i + \sum_i^{n_{\text{pix}}} R_i + \sum_i^{n_{\text{pix}}} U_i \quad (2)$$

The classical derivation concludes at these noise terms. The classical formulation of the CCD equation hence results in the following expression:

$$\begin{aligned} \text{SNR}_{\text{classical}} &= \frac{S^*}{\sqrt{S^* + n_{\text{pix}} \cdot (S_{\text{S}}^* + N_{\text{D}}^2 + N_{\text{R}}^2 + N_{\text{U},i}^2)}} \quad (3) \\ &= \frac{\sum_i^{n_{\text{pix}}} \lambda_{\text{obj},i}}{\sqrt{\sum_i^{n_{\text{pix}}} \lambda_{\text{obj},i} + n_{\text{pix}} \cdot (\lambda_{\text{S}} + \lambda_{\text{D}} + N_{\text{R}}^2 + \frac{g^2}{24})}} \end{aligned}$$

Remarks:

- $\frac{g^2}{24}$ is the truncation noise modelled as a uniform random variable support $[-\frac{g}{2}, \frac{g}{2}]$
- N_{R}^2 is the readout noise
- λ_{S} and λ_{D} are the background noise and the dark noise

Note that the noise introduced by the subtraction of the background to the is not accounted for. Merline introduces an additional noise term, that stems from the generation of the background level:

$$B = \frac{1}{n_{\text{B}}} \sum_i^{n_{\text{B}}} (S_{\text{S},i} + D_i + R_i + U_i) \quad (4)$$

Where B is the background subtraction term and n_{B} is the number of background pixels used to estimate the background. Denoting the standard deviation of the background estimation noise as $N_{b,d} = \text{Var}(B)$ the noise variance becomes :

$$N_{\text{Merline}}^2 = N_{\text{classical}}^2 + \frac{n_{\text{pix}}}{n_{\text{B}}} N_{b,d}^2 \quad (5)$$

Leading to the modified CCD equation of Merline:

$$\text{SNR}_{\text{Merline}} = \frac{S^*}{\sqrt{S^* + n_{\text{pix}} \left(1 + \frac{1}{n_{\text{b}}}\right) (S_{\text{S}}^* + N_{\text{D},i}^2 + N_{\text{R},i}^2 + N_{\text{U},i}^2)}} \quad (6)$$

The modification introduced in [MH95] leads to the addition of $\frac{n_{\text{pix}}}{n_{\text{b}}} (S_{\text{S}}^* + N_{\text{D},i}^2 + N_{\text{R},i}^2 + N_{\text{U},i}^2)$ in the noise estimation with respect to the classical one.

Discussion of the Hypotheses of the Classical and Merline CCD Equation

In our updated formulation the following hypotheses are dropped.:

The truncation noise is an independent additive uniform noise: During the truncation process the signal is converted from electrons into ADU. This conversion leads to lost in resolution: the CCD can only count a number of electrons at the time. This assumption is conceptually wrong and leads to inaccurate estimations of the truncation noise for faint signals (cf section III for more details), besides it entails that the signal remains a Poisson distribution after the round off error.

The number of signal pixels is perfectly known: As with the background estimation, the number of pixels that belong to the object is determined as the number of pixels above the background level. Especially for very faint signals this assumption is problematic (see Fig 1). In fig ??, the problem of ambiguous pixels is exemplified. Schematic (a) presents a case where there are no ambiguous pixels. Schematic (b) presents a case where some pixels may belong either to the signal or the background. In this case, it may be impossible to tell signal pixels from background pixels. This issue will be assessed in the derivation of the improved CCD equation in the following section.

2.1. Derivation under more general conditions

In the improved derivation of the CCD equation is based upon the derivation from [MH95]. The modelling of the truncation error is improved upon and the uncertainty in the number of object pixels is taken into account. Improvements are most significant for faint object signals. In this section we denote $S_{act,i} = S_{obj,i} + S_{S,i} + D_i$ the number of electrons collected at pixel i that will be converted into ADU (Analog to Digital Unit).

First, we compute the exact distribution of the signal after electron to ADU conversion. Let's assume g is the number electrons corresponding to one ADU. For the sake of simplicity we assume that g is even and noting $S_{act,i}^r$ the new distribution in ADU, we get for the probability of the signal in ADU of an original signal in the interval subject to truncation, for any signal strength q :

$$P(S_{act,i}^r = q) = P\left(S_{act,i} \in \left[g\left(q - \frac{1}{2}\right); g\left(q + \frac{1}{2}\right)\right]\right) \quad (7)$$

for any $q > 0$.

This is equivalent to:

$$\begin{aligned} P(S_{act,i}^r = q) &= \sum_{k=gq}^{g(q+1)-1} \frac{\exp(-\lambda_{tot,i}) \lambda_{tot,i}^{k-\frac{1}{2}g}}{(k - \frac{g}{2})!} \\ &= \frac{\Gamma(g(q + \frac{1}{2}), \lambda_{tot,i})}{\Gamma(g(q + \frac{1}{2}))} - \frac{\Gamma(g(q - \frac{1}{2}), \lambda_{tot,i})}{\Gamma(g(q - \frac{1}{2}))}, \end{aligned} \quad (8)$$

for any $k > 0$, with $\Gamma(q) = (q - 1)!$ is the Gamma

function and $\Gamma(q, x) = \int_x^\infty e^{-t} t^{q-1} dt$ is the incomplete Gamma function.

Fig 1 gives an example of very faint signal where the pixel at the edge are extremely ambiguous. Ambiguous pixels are those that could be part of the signal or part of the background. In [MH95, New91] or the classical equation, the ambiguous pixels are neglected. Our CCD equation accounts for the ambiguous pixels that can be part of the signal and of the background determination. We denote I_{amb} the set of ambiguous pixels. The ambiguous pixels are included in the background determination and are considered as being part of the signal. In other words, we have $I_{amb} \in I_{sig}$ and $I_{amb} \in I_B$, where I_{sig} is the set of signal pixels from the object trace and I_B is the set of background pixels used in the background determination. We denote the overall actual signal as S_{act} (signal, dark noise and background). Following the derivation described in [SF16a], the CCD equation becomes:

$$\begin{aligned} \text{SNR}_{\text{impro}} &= \frac{S^*}{\sqrt{(n_{\text{pix}} - \frac{2n_{amb}n_{\text{pix}}}{n_B} + \frac{n_{amb}n_{\text{pix}}^2}{n_B^2})(N_{act}^r)^2}} \quad (9) \\ &= \frac{S^*}{\sqrt{(\frac{n_{\text{pix}}}{n_B})^2(n_B - n_{amb})(N_{d,b}^r)^2 + nN_R^2}} \quad (10) \end{aligned}$$

Where $N_{b,d}^{r2}$ is the variance of the (truncated) background signal. N_{act}^{r2} is the variance of the (truncated) signal in pixels the object trace. Further simplifications can be made in the case the number of signal pixels is much smaller than the amount of pixels used for the background determination. In that case, the ratio $\frac{n_{amb}}{n_B}$ is going to be very small as the background will be very well determined. In this case we can take $\frac{n_{amb}}{n_B} \rightarrow 0$ in Eq. 10. Besides, if the truncation noise is modelled, the traditional way, then Eq. 10 gives Merline's CCD equation. Note that the presence of ambiguous pixels affects the effective number of pixels to consider in the noise estimation while the accurate truncation modelling transforms the shape of the distribution. Contrary to the previous CCD equations, the signal distribution is not Poisson distributed anymore. Note that the modelling of ambiguous pixels tends to reduce to noise. This come from the fact that some pixels are at the same time in the background estimation and the signal.

3. PERFORMANCE OF THE IMPROVED CCD EQUATION

In order to evaluate the effects of different CCD equations, CCD frames are numerically simulated in order to compare the CCD equations. To do so a Gaussian noiseless signal is generated and constant background noise is added to it. Then an artificial CCD reads the signal and adds noise to it. The Gaussian signal is then read multiple times yielding different observations of the same

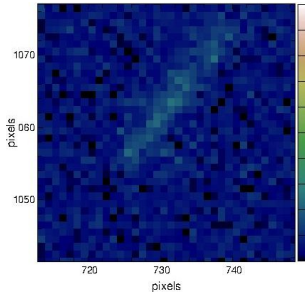
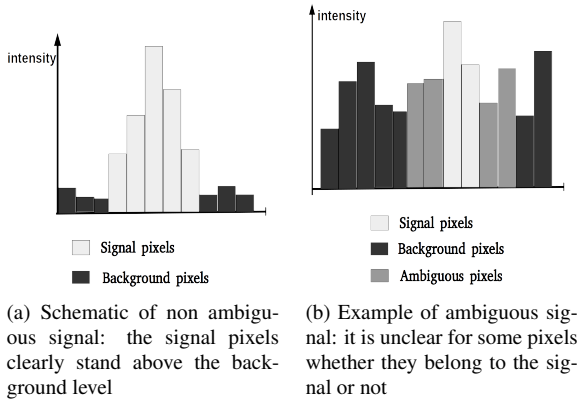


Figure 1: example of a very faint signal with low signal to noise ratio

object so the noise can be estimated using Monte Carlo method. The numerical results are then compared to the three CCD equations derived in the previous section Eq.4, Eq.6 and Eq.10.

3.1. Comparison of the Signal to noise ratio for signals without ambiguous pixels

The different formulations of the CCD equation are compared to Monte Carlo simulations. The following results are obtained including all sources of noise described in the introduction. In the first case, it is assumed that the signal pixels are perfectly identified. To illustrate Fig 6b shows an example of signal in which the object pixels can be easily identified, as the signal to noise ratio in all object pixels is high. Fig 2 shows three different estimations of the signal to noise ratio: the classical CCD equation, Merline's CCD equation as presented in [MH95] and the improved CCD equation. All three are compared to a Monte Carlo estimation of the Signal to noise ratio. Merline is extremely accurate even with a high gain and it almost equivalent to the CCD equation presented in the last section. The classical equation (Eq. 4) overestimates the signal to noise as it does not take into account the background subtraction.

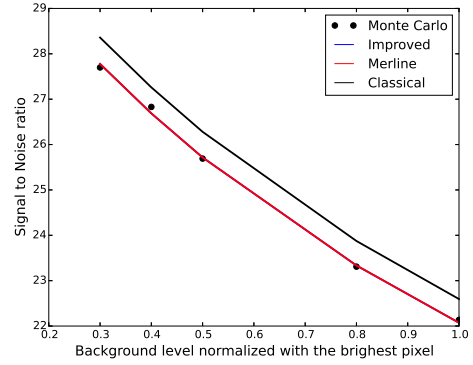


Figure 2: Evolution to signal to noise ratio with read out noise. In this case $g = 0.06\lambda_{obj}$

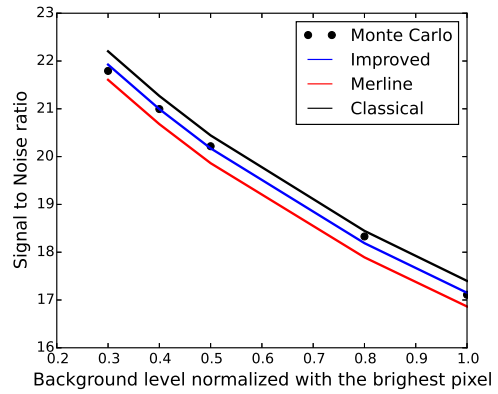


Figure 3: Evolution to signal to noise ratio with the background level.

3.2. Comparison of the Signal to noise ratio for signals with ambiguous pixels

In this case, we take into account the presence of ambiguous pixels. As the signal can be extremely faint, it may become extremely difficult to tell whether a pixel belongs to the background or the signal. Furthermore, in some cases, where very few pixels are available to compute the background, one has to include those ambiguous pixels in their estimation of the background level. In practice, the ambiguous pixels are pixels for which the intensity from the observed object is of the same order of magnitude as the background noise. Fig 3 shows that [MH95] underestimate the signal to noise ratio as they neglect the correlation between the background estimation and the signal due to the presence of ambiguous pixels.

The difficulty behind differentiating the signal pixels from the background pixels makes the classical definition of the signal to noise ratio extremely ambiguous and subject to the observer subjectivity. In the next section, we present an alternative definition of the signal to noise ratio that does not present this ambiguity.

3.3. Alternative definition of the signal to noise ratio based on the brightest pixel

The presence of ambiguous pixels that could be part of the signal as well as the background creates difficulties when computing the signal to noise ratio. We propose an alternative definition of the signal to noise ratio which is easier to assess in the case of a faint signal with ambiguous pixels. This definition circumvent the problem of ambiguous pixels as the signal of the brightest pixel is readily extracted and unambiguous. As the influence of the truncation error is small, this new definition recreates the situation of Fig 2 and allows to use Merline's CCD equation with a high level of accuracy.

4. PROBABILITY OF DETECTION

The probability of detection denotes the a priori probability that a given object is detected. In our framework, the probability of detection is defined relative to the brightest pixel. The reasoning is, that if the brightest pixel of an object is below detection limit, the object will not be detected. This does not include to evaluate the probability of detection after e.g. a spatial filter has been applied. Introducing the threshold t , the signal can be detected if at least one signal pixels has intensity greater than the threshold t . Therefore we have:

$$P(\text{detection}) = P(S_{\text{brightestpixel}}^r > t) + P(S_{\text{brightestpixel}}^r < t \text{ at least one other } j \text{ has } S_j > t), \quad (11)$$

where $S_{\text{brightestpixel}}^r$ is the intensity of the expected brightest pixel. It is the intensity measured and therefore is comprised of the signal itself and the background noise both truncated plus the readout noise. In practice, if the brightest pixel is clearly brighter than the other signal pixels, the second term is very small as it is very unlikely that one does not detect the expected brightest pixel but detect a lower expected intensity pixel. In the following derivation, we focus only on the brightest pixel. Therefore we have

$$P(\text{detection}) = 1 - P(S_{\text{brightestpixel}}^r < t). \quad (12)$$

For the rest of the derivation it implicit that only the brightest pixel is considered. From the previous section we have

$$S_{\text{brightestpixel}}^r = S_{\text{act}}^r - B + S_R \quad (13)$$

Where S_{act}^r is defined in the previous section, B is the background estimation and S_R represent the read out noise. If we use the signal distribution derived in the previous section, we have:

$$P(\text{detection}) = 1 - P(S^r - B + S_R < t). \quad (14)$$

Computing $P(S^r - B + R < t)$ can be complex and numerically expensive. Reasonable simplifications are proposed in order to explicate $P(S^r - B + R < t)$. Assuming that the background estimation is Gaussian distributed and using the definition of the truncated signal

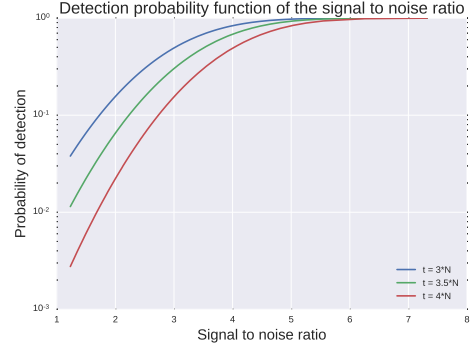


Figure 4: Detection probability function of the signal to noise ratio

distribution, the probability of detection can be written as : [SF16a]

$$P(\text{detection}) = 1 - \frac{1}{2} \sum_{n=-\infty}^{\infty} \frac{\Gamma(n - \frac{q}{2}, \lambda_{\text{obj}} + \lambda_S + \lambda_D)}{n!} \cdot \left(\text{erf} \left(\frac{n + 1 - t - \mu_B}{\sqrt{2g(\sigma_B^2 + \sigma_R^2)}} \right) - \text{erf} \left(\frac{n - t - \mu_B}{\sqrt{2g(\sigma_B^2 + \sigma_R^2)}} \right) \right). \quad (15)$$

Where erf is the error function.

Eq. 15 can be evaluated numerically for different signal to noise ratios. As the choice of t is not unique, the results are plotted on Fig 4 for different values of t . t is chosen as $k \times N$, where N is the noise. The value of the threshold should be chosen such as it minimizes the risk of false detection and maximize the number of space objects detected. Therefore its value is specific to the sensor signal to noise ratio and enhancement methods that have been applied in the image processing step.

5. ESTIMATING THE OBJECT POSITION AND QUANTIFYING THE UNCERTAINTY IN THE ESTIMATION

In this section a position estimation method is presented, based on the Gaussian fitting of the CCD signal. The results of this section are further explained in [SF16b] The Airy disk refraction pattern at the sensor is fitted with a Gaussian shape. For details see [FJ14]. The actual position of the source can be retrieved under the assumption that it corresponds to the center of the fitted Gaussian curve on the pixel grid. More precisely, assuming the ground signal has the following form

$$s = A e^{-\frac{1}{2}(c_1(x_i - x_0)^2 + 2c_3(x_i - x_0)(y_i - y_0) + c_2(y_i - y_0)^2)}, \quad (16)$$

And noting $\theta = (A, x_0, y_0, c_1, c_2, c_3)$ where A is the amplitude, x_0 and y_0 the center of the Gaussian and c_1, c_2

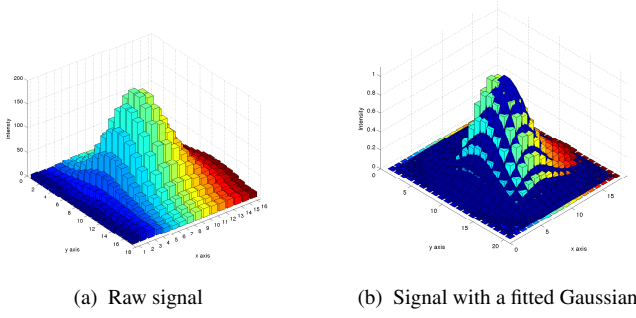


Figure 5: Gaussian curve fitted to an actual space object signal.

and c_3 the coefficients of the inverse covariance matrix. Then the position of the object is x_0, y_0 .

The angles can be given in arcsec. c_1, c_2, c_3 are expressed in arcsec^{-2} and A is a number of electron per arcsec^2 . The pixel scale (arcseconds per pixel) is assumed to be known; it is also needed to determine the amount of irradiation that is collected in each of the pixels containing signal from either the object or the background. The aim is to find x_0 and y_0 using the noisy signal issued by the CCD in subpixel accuracy. In this section, the signal measured by the CCD at pixel i is noted g_i . An example of Gaussian fitting applied to an actual signal is given in Fig. 5.

5.1. The maximum of likelihood estimation

The maximum of likelihood (ML) estimator has been widely used in Gaussian fitting of signals [Sal74, Win86, HD08] for its good properties: it is an unbiased, consistent and asymptotically efficient estimator [SO09]. Defining the likelihood of the set of parameters θ for a signal as:

$$L = P(S = s|\theta). \quad (17)$$

Then the maximum of likelihood is defined as:

$$\hat{\theta}_{MLE} = \max_{\theta} (P(S = s|\theta)). \quad (18)$$

In the first section of this study S has been defined as: $S = \sum_i S_{i,\text{act}}^r + S_{i,\text{R}} - B$ The likelihood function for pixel i can be rewritten as

$$L_i = P(S_i = s_i|\theta) = P(S_{i,\text{act}}^r + S_{i,\text{R}} - B = s_i|\theta) \quad (19)$$

Under the assumption that the number of pixel for the background is large (hypothesis 1), the CCD resolution is high (small gain) (hypothesis 2) and the signal is bright, the signal is Gaussian distributed [SF15]:

$$S_i = \lambda_{\text{act},i} - \lambda_{b,d} + \mathcal{N}\left(0, 1_s \times \sqrt{\lambda_{\text{act},i} + \frac{\lambda_b}{n_b} + \sigma_R^2}\right). \quad (20)$$

Assuming that the signal is a Gaussian curve (hypothesis 4):

$$\begin{aligned} \lambda_{\text{act},i} - \lambda_{b,d} &= \lambda_S \\ &= \delta_x \delta_y A e^{\left(-\frac{1}{2}(c_1(x_i - x_0)^2 + 2c_3(x_i - x_0)(y_i - y_0) + c_2(y_i - y_0)^2)\right)}. \end{aligned} \quad (21)$$

with x_i, y_i , being the center coordinates of pixel i , δ_x, δ_y is the size of the pixel in arcsec^{-1} in the x- and y direction of the pixel grid, respectively. In the remainder $\sigma_i^2 = \lambda_{\text{tot},i} + \frac{\lambda_b}{n_b} + \sigma_R^2$ denotes a number of electrons in the energy equivalent.

Consequently, if the noise is independent for two different pixels, the likelihood becomes:

$$L = \prod_i^{n_{\text{pix}}} \exp\left(-\frac{1}{2} \left(\frac{(g_i - s_i)^2}{\sigma_i^2}\right)\right). \quad (22)$$

s_i has been defined in Eq. 16, and g_i intensity measured at pixel i . Then the log likelihood also called the score is:

$$l = -\sum_i^{n_{\text{pix}}} \frac{(g_i - s_i(\theta))^2}{2\sigma_i^2}. \quad (23)$$

Then l has to minimize to get θ_{MLE} .

5.2. Quantification of the uncertainty in the estimation

In this section, an estimation is given for the variance in the pixel position estimation of the space object. Two different approaches to quantify the uncertainty in the estimation of the parameters are: a maximum of likelihood estimation as it is carried in [HD08, BDL07] or a Bayesian approach as in [SO07]. Both methods tackle a problem from a different angle so the uncertainty in the estimation are in general different. The maximum of likelihood estimation focuses on estimating the deterministic parameters θ_{true} and then estimates the uncertainty in the estimator $\hat{\theta}$. On the contrary, with the Bayesian approach one considers the distribution of Θ for a given set of measurements. Therefore, even if non informative priors are used for the Bayesian estimation both cases are not exactly equivalent. The Bayesian estimation gives all the possible values of θ corresponding to the observed object image.

Rao-Cramer lower bound Under regularity assumptions on the likelihood function, for any unbiased estimator, there exists a variance lower bound [SO09]. In our case, the Maximum of Likelihood (ML) estimator asymptotically reaches this lower bound [SO09, BM13]. We introduce the Fisher information as:

$$F(\theta) = E \left[\frac{\partial^2 l}{\partial^2 \theta_i \theta_j} \right], \quad (24)$$

where $\theta = (A, x_0, y_0, c_1, c_2, c_3)$, l is defined in Eq. 23 and E is the expected value with respect to the likelihood. As explained in [SO09], the Fisher information corresponds to the average amount of information available in the sample. The Rao Cramer variance lower bound follows the following inequality:

$$\text{Var}_{g_1 \dots g_n}(\hat{\theta}) \geq F(\theta)^{-1}. \quad (25)$$

And if the sample size is large enough, the ML estimator asymptotically can be represented with a Gaussian distribution ([BDL07, BM13]):

$$\hat{\theta} \sim \mathcal{N}(\theta_{\text{true}}, F(\theta)^{-1}). \quad (26)$$

In practice, if the number of sample is large, the lower bound will be reached and the inequality becomes an equality. For well sampled cases, it provides an analytical expression of the variance.

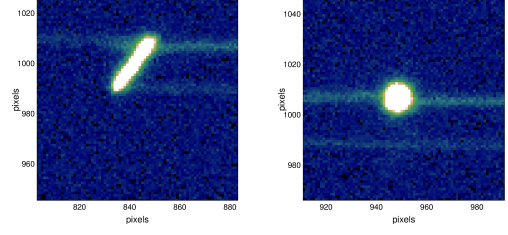
In many cases, simple analytical expression of the Fisher information are not available, but in this case previous work [HKD07, HD08] have managed to derive such expression under the following assumptions:

1. Flat noise: σ is constant over all pixels of the signal.
2. The profile is well sampled: the pixel size is constant and small compared to the object image size. In other words we have $\delta_x, \delta_y \ll \frac{1}{c_1^{0.5}}, \frac{1}{c_2^{0.5}}$ where δ_x and δ_y are the CCD pixel dimensions.
3. The entire profile of the object image is sampled

In our work however we were able to drop the third assumption. Detailed calculation of the RCLB are displayed in [SF16b]. It can finally be shown that for a cropped image between $[x_0 - a; x_0 + a] \times [y_0 - b; y_0 + b]$, the object position covariance matrix becomes :

$$\begin{aligned} K_{x_0, x_0} &= 2\sigma^2 \frac{c_1 c_2 \sqrt{\pi} + 2 c_1 c_2 \sqrt{\frac{D}{c_2}} a d_a + 2 \sqrt{\frac{D}{c_1}} b c_3^2 d_b}{\pi^{3/2} \sqrt{D} A^2 c_1} \\ K_{x_0, y_0} &= -2\sigma^2 \frac{c_3 \left(\sqrt{\pi} + 2 \sqrt{\frac{D}{c_2}} a d_a + 2 \sqrt{\frac{D}{c_1}} b d_b \right)}{\pi^{3/2} \sqrt{D} A^2} \\ K_{y_0, y_0} &= 2\sigma^2 \frac{c_1 c_2 \sqrt{\pi} + 2 c_1 c_2 \sqrt{\frac{D}{c_1}} b d_b + 2 \sqrt{\frac{D}{c_2}} a c_3^2 d_a}{\pi^{3/2} \sqrt{D} A^2 c_2} \end{aligned} \quad (27)$$

c_1 and c_2 are parameters of the fitted Gaussian curve that quantify the size of the signal in x and y direction. c_3 accounts for the orientation of the signal with respect to the axes. A is the intensity of the brightest pixel. D is defined as $D = c_1 c_2 - c_3^2$. $d_a = \exp\left(-\frac{D a^2}{c_2} D\right)$ and $d_b = \exp\left(-\frac{D b^2}{c_1} D\right)$ accounts for the truncation of the signal. If the complete object image would be able to be sampled d_b and d_a go to zero and the variance simplifies



(a) Signal in the general case where $c_1 \neq c_2$ and $c_3 \neq 0$ (source ZIM-LAT,AIUB) (b) Example of rotation invariant signal where $c_1 = c_2$ and $c_3 = 0$ (source ZIM-LAT,AIUB)

Figure 6: Signals received from an object

into the results developed in [HD08]. In realistic settings, finite cropping has to be applied.

Eq. 27 can be further simplified, by noticing that

$$\frac{S_b}{N} = \frac{A \exp\left(-\frac{1}{2}(c_1 u_x^2 + 2c_3 u_x u_y + c_2 u_y^2)\right) \delta_x \delta_y}{\sigma}, \quad (28)$$

u_x and u_y were previously defined as the minimum distance between the center of the Gaussian surface and the center of a pixel for a given signal. Eq. 29 does not take into account the pixel integration. It is possible to average u_x and u_y as in the derivation of the Rao Cramer Lower Bound, however, to simplify u_x and u_y are set to zero so Eq. 28 becomes:

$$\frac{S_b}{N} = \frac{A \delta_x \delta_y}{\sigma}, \quad (29)$$

and Eq. 27 becomes:

$$\begin{aligned} K_{x_0, x_0} &= \frac{2c_2 \left(\sqrt{\pi} + 2 \sqrt{\frac{D}{c_2}} a d_a + 2 \sqrt{\frac{D}{c_1}} \rho^2 b d_b \right) \delta_x \delta_y}{(S_b/N)^2 \sqrt{D} \pi^{3/2}} \\ K_{x_0, y_0} &= \frac{-2c_3 \left(\sqrt{\pi} + 2 \sqrt{\frac{D}{c_2}} a d_a + 2 \sqrt{\frac{D}{c_1}} b d_b \right) \delta_x \delta_y}{(S_b/N)^2 \sqrt{D} \pi^{3/2}} \\ K_{y_0, y_0} &= \frac{2c_1 \left(\sqrt{\pi} + 2 \sqrt{\frac{D}{c_1}} b d_b + 2 \sqrt{\frac{D}{c_2}} \rho^2 a d_a \right) \delta_x \delta_y}{(S_b/N)^2 \sqrt{D} \pi^{3/2}} \end{aligned} \quad (30)$$

where $\rho = \frac{c_3}{\sqrt{c_1 c_2}}$ is a correlation factor between the x and y axis. It defines the orientation of the (elongated) Gaussian with respect to the pixel grid.

If the signal is rotation invariant as in Fig 6b then $c_1 = c_2 = c$ and $c_3 = 0$ Eq. 30 becomes: Introducing the signal to noise ratio as defined in Eq. 29 and assume square pixels, we get:

$$\begin{aligned} K_{x_0, y_0} &= \frac{\delta^2}{\pi^{3/2} (S_b/N)^2} \times \\ &\begin{bmatrix} 2(\sqrt{\pi} + 2\sqrt{c} a d_a) & 0 \\ 0 & 2(\sqrt{\pi} + 2\sqrt{c} b d_b) \end{bmatrix}. \end{aligned} \quad (31)$$

Even in the symmetrical case we see that x_0 and y_0 are not uncorrelated due to the nuisance parameters.

5.3. Method Comparison and Evaluation

The different methods for evaluating the variance in the object image centroid on the pixel frame are compared: The simplified method according to [HD08] using the Rao Cramer Lower Bound (RCLB), the improved method to computing the RCLB introduced in this paper, and the Bayesian estimation. As ground truth a Monte Carlo simulation is used with 1000000 samples. For the Bayesian estimation, a Markov Chain Monte Carlo (MCMC) based on Metropolis algorithm [MRR⁺53] method is used to compute the posterior distribution using 100000 samples. Presentation of the method are presented in [KS05]. The results for t noise levels SNR=30 (relative to the brightest pixel) are shown in Fig.7, in dependence of the full width at half maximum (FWHM) of the object image. The variance is given in pixels². The object image has been cropped at 2 standard deviations in x direction and 2.5 standard deviation in y direction, the noise is assumed to be constant over this cropped subframe. For instance, if the standard deviation of the fitted Gaussian is 5 pixels in x and y direction, in our test case the cropped image will be centered around the signal, 40 pixels large in x direction and 50 pixels wide in y direction. It can be seen that the approximation of the RCLB according to [HD08] constantly underestimates the variance, and is hence overconfident. Although a priori, the RCLB underestimates the variance of the ML estimator, Fig. 7 shows that in practice it is reached even for object images with very small FWHM with the improved method, even in cases with a low signal to noise ratio. Consequently, even for those (FWHM e.g 10 pixels) the approximate RCLB defined in Eq. 27 is a good estimation of the variance. Using the exact expressions for the RCLB (obtained by taking the inverse of the matrix in Eq.?? only shows significant improvements for object images with FWHM lower than two pixels. Non surprisingly, for those cases the variance sharply increases, as more and more information is integrated into practically one pixel.

The computationally more expensive method of the Bayesian approach agrees with the results given by the Monte Carlo computations. Beside for signals larger than ten pixels the analytical expression for the parameter variance (Eq. ??) fairly well agrees with the Bayesian results. This result confirms that Eq. ?? is a valid estimation of the uncertainty in astrometric estimation.

6. CONCLUSIONS

In this study probability of detection and position uncertainty were analytically derived. Different versions of the CCD equation were compared with Monte Carlo simulations, showing that Merline's CCD equation provides a good estimation of the signal-to-noise ratio

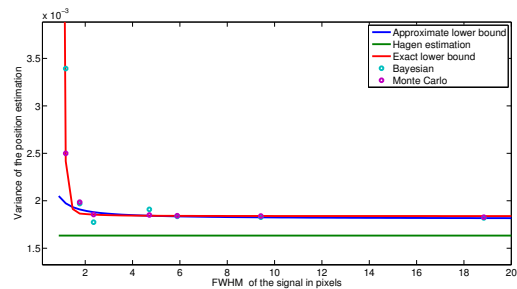


Figure 7: Convergence of the ML position estimation variance for generated signal with SNR=30

(SNR) in the case of well-defined signals. However, in the presence of ambiguous pixels, the improved CCD equation performs significantly better. Using the full distribution of CCD output signal (sum of a truncated Poisson and the Gaussian), the probability of detection was derived in a general context and it was shown that it directly depends on the SNR of the brightest pixel and the detection threshold. Those results can directly be implemented in multi-target tracking algorithms to accurately evaluate the probability of detection knowing only the signal-to-noise ratio and the detection threshold. An analytical expression for the astrometric position variance of non-resolved CCD sources were derived in this paper. It shows that the observation likelihood can be computed fully analytically solely based on the physical quantities of the Gaussian shape of the non-resolved source, the SNR and the pixel size. This saves the computationally expensive generation of an artificial observation frame and its Gaussian fitting, or other numerical methods. Using a Bayesian approach, it was also shown that the distribution of the position estimation is well described by its first two moments. For the case of real observations, where the signal geometry is not precisely known a priori, a simple lookup table allows to determine variances and probability of detection based on pixel values, without numerical procedures. Alternatively, Gaussian fitting on the real image can be performed in order to have a precise knowledge of the geometry of the signal and compute the position uncertainty via the derived analytical expression.

REFERENCES

- BDL07. Harrison H Barrett, Christopher Dainty, and David Lara. Maximum-likelihood methods in wavefront sensing: stochastic models and likelihood functions. *JOSA A*, 24(2):391–414, 2007.
- BM13. H H Barrett and K J Myers. *Foundations of Image Science*. Wiley Series in Pure and Applied Optics. Wiley, 2013.
- CF08. Delande Daniel Clark, Emmanuel and Carolin Frueh. Multi-Object Filtering for Space Situational Awareness. Technical report, Heriot-Watt University, Edinburgh, 2008.

- DFHC15. E D Delande, C Frueh, J Houssineau, and D E Clark. Multi Object Filtering for Space Situational Awareness. *AAS Space Flight Mechanics Meeting*, 2015.
- DHF⁺15. Kyle J DeMars, Islam I Hussein, Carolin Frueh, Moriba K Jah, and R Scott Erwin. Multiple-Object Space Surveillance Tracking Using Finite-Set Statistics. *Journal of Guidance, Control, and Dynamics*, pages 1–16, 2015.
- FJ14. Carolin Frueh and Moriba Jah. Detection Probability of Earth Orbiting Objects Using Optical Sensors. In *Advances in the Astronomical Sciences*, Hilton Head, 2014.
- HD08. Nathan Hagen and Eustace L Dereniak. Gaussian profile estimation in two dimensions. *Applied optics*, 47(36):6842–6851, 2008.
- HKD07. Nathan Hagen, Matthew Kupinski, and Eustace L Dereniak. Gaussian profile estimation in one dimension. *Applied optics*, 46(22):5374–5383, 2007.
- KS05. Jari Kaipio and Erkki Somersalo. *Statistical and Computational Inverse Problems*, volume 160 of *Applied Mathematical Sciences*. Springer-Verlag, New York, January 2005.
- Mas92. George H. Massey, Philip Jacoby. CCD Data: The Good, The Bad, and The Ugly. In Steve B. Howell, editor, *Astronomical CCD observing and reduction techniques*, volume 23, page 240, San Francisco, 1992. Astronomical Society of the Pacific.
- MDF15. James S McCabe, Kyle J DeMars, and Carolin Frueh. Integrated Detection and Tracking for Multiple Space Objects. *AAS Space Flight Mechanics Meeting*, 2015.
- MH95. W J Merline and Steve B Howell. A realistic model for point-sources imaged on array detectors: The model and initial results. *Experimental Astronomy*, 6(1-2):163–210, 1995.
- MRR⁺53. Nicholas Metropolis, Arianna W. Rosenbluth, Marshall N. Rosenbluth, Augusta H. Teller, and Edward Teller. Equation of State Calculations by Fast Computing Machines. *The Journal of Chemical Physics*, 21(6):1087, 1953.
- New91. Michael V. Newberry. Signal-to-noise considerations for sky-subtracted CCD data. *Astronomical Society of the Pacific*, 103:122–130, 1991.
- Sal74. Bahaa E A Saleh. Estimation of the Location of an Optical Object with Photodetectors Limited by Quantum Noise. *Appl. Opt.*, 13(8):1824–1827, August 1974.
- SF15. Francois Sanson and Carolin Frueh. Noise Quantification in Optical Observations of Resident Space Objects for Probability of Detection and Likelihood. In *Proc. AIAA/AAS Astrodynamics Specialist Conference*, Vail, Colorado, 2015.
- SF16a. F. Sanson and C. Frueh. Probability of detection in non-resolved images: Application to space object observation. *Journal of Astronomical Sciences*, submitted, 2016.
- SF16b. F. Sanson and C. Frueh. Space object position uncertainty quantification in non-resolved images. *IEEE Transactions on Aerospace and Electronic Systems*, submitted, 2016.
- SO07. Richard S Savage and Seb Oliver. Bayesian methods of astronomical source extraction. *The Astrophysical Journal*, 661(2):1339, 2007.
- SO09. A Stuart and K Ord. *Kendall's Advanced Theory of Statistics: Volume 1: Distribution Theory*. Number vol. 2; vol. 1994 in Kendall's Advanced Theory of Statistics. Wiley, 2009.
- Tie93. Heinz Tiersch. S.B. Howell (ed.): Astronomical CCD observing and reduction techniques. Astronomical Society of the Pacific 1992, ASP Conference Series 23, 339 s., Preis: 55,-ISBN 0-937707-42-4. *Astronomische Nachrichten*, 314(6):398, 1993.
- Win86. Kim A Winick. Cramer-Rao lower bounds on the performance of charge-coupled-device optical position estimators. *JOSA A*, 3(11):1809–1815, 1986.